

Gaussian filter-based dark channel prior for image dehazing enhancement

Oky Dwi Nurhayati¹, Bayu Surarso², Wahyul Amien Syaifei², Dinar Mutiara Kusumo Nugraheni²

¹Department of Computer Engineering, Diponegoro University, Semarang, Indonesia

²Master Program of Information System, Diponegoro University, Semarang, Indonesia

Article Info

Article history:

Received Apr 13, 2024

Revised Jul 11, 2024

Accepted Jul 17, 2024

Keywords:

Dark channel prior

Gaussian filter

Hazy images

Image dehazing

Single-image dehazing

ABSTRACT

The presence of haze in an image is one of the challenges in computer vision tasks, such as remote sensing, object monitoring, and traffic monitoring applications. The hazy image is considered to contain noise and it can interfere with the image analysis process. Thus, image dehazing becomes a necessity as part of image enhancement. Dark channel prior (DCP) is one of the images dehazing methods that works based on a physical degradation model and utilizes low-intensity values from outdoor image characteristics. The DCP method generally consists of some steps, which are finding the dark channel and gradient image, estimating the sky region, atmospherical light, and transmission map, and reconstructing the dehazed image. This study introduces image dehazing by utilizing the Gaussian filter combined with the DCP method to increase the sharpness and accentuate the details of hazy images. Experimental results show that the proposed method could produce dehazed images with a visual quality is 18.94 dB on average or an increase of 11.91% compared to the original hazy image with a similarity index is 66.71% on average or an increase of 8.10%. Therefore, it is expected that this study can contribute to the image dehazing method enrichment based on DCP.

This is an open access article under the [CC BY-SA](https://creativecommons.org/licenses/by-sa/4.0/) license.



Corresponding Author:

Oky Dwi Nurhayati

Department of Computer Engineering, Diponegoro University

Semarang 50275, Indonesia

Email: okydwin@gmail.com

1. INTRODUCTION

Image is one of the substantial inputs in computer vision tasks. For understanding and interpreting visual information with reliable accuracy, computer vision applications require a high-quality input image, such as safety monitoring, remote sensing, autonomous driving assistance, surveillance, video analysis, image classification, image segmentation, object detection, radar tracking, behavior analysis, and aerial imaging [1]–[8]. However, input images from the acquisition are sometimes not always able to produce a high-quality input image. In the case of outdoor images that are captured in an outdoor environment, there are many factors to produce a high-quality image acquisition. Several factors may be controllable, such as a camera, lens, sensor, and also a photographer. Providing good quality devices with the right settings and supported by expertise in photography will help to produce a high-quality image acquisition. Nevertheless, there is also an uncontrollable factor, such as weather or atmospherical conditions. Outdoor image captured in bad or poor weather conditions often has low quality due to the presence of particle pollution in the atmosphere such as fog or haze, dust, smoke, water droplets, and other conditions affected by aerosols [1], [2], [4], [9], [10]. The hazy images affect the brightness, contrast, and sharpness, and it usually has an impact on the accuracy level of analysis [4], [11].

Dealing with this importance, image dehazing become a popular task in computer vision as an image preprocessing to improve the image visually by reducing or removing the effect of haze that covers the image [1], [2]. Image dehazing will enable computer vision analysis from low-level interpretation toward high-level understanding. There are numerous image dehazing methods have been proposed to reduce or remove the haze effect from an image. Those methods have their characteristics, assumptions, and constraints. Image dehazing is generally undertaken using the atmospheric scattering model (ASM) from hazy images [12]. Based on the number of input hazy images, the image dehazing methods can be categorized into two types that are multiple and single image dehazing [1], [13]. The multiple-image dehazing works with several hazy images of the same scene to map to its dehazed image, while the single-image dehazing technique works with only one hazy image used to map to its dehazed image. In multiple-image dehazing, a dehazed image is recovered from hazy images based on the different polarizing filters using a degree of polarization, and different weather conditions [14]–[17] to overcome the effects of poor weather. Another approach in multiple-image dehazing is proposed using additional segmentation to follow the change of scene in multiple-image dehazing [18]. The use of multiple inputs of hazy images can provide a variety of different information that can complement each other. It will be expected to lead to a benefit on dehazing processes, such as estimation of transmission map and atmosphere light to produce a better dehazing image quality. However, this dehazing type has some difficulties to implement practically, such as the availability of different images in the same scene in a short time, computational complexity, dependencies between input images, and special device requirements [1], [15]. To deal with these limitations, a single-image dehazing method got a lot of attention from many studies to get a better dehazed image because this method is more realistic in practice through a more efficient process [19]–[21].

Based on these considerations, this study will focus on hazy image enhancement on the single image dehazing approach. Single-image dehazing uses one hazy image with a priori assumptions that emphasize the additional information or prior knowledge to obtain the dehazed image [15], [21]. There are some single-image dehazing techniques based on prior knowledge have been proposed over recent years. Earlier, Tan [22] proposed single-image dehazing using two prior assumptions based on contrast and attenuation. It was assumed that the contrast of the hazy-free image is higher than that of the hazy image. Besides, the attenuation of the spots should be smooth and it is assumed as a continuous function of distance. This method can maximize local contrast using one haze image but cause a halo effect [15]. Further, Fattal [23] proposed three steps for image dehazed, which are estimating the surface albedo, obtaining the medium transmission, and recovering the hazy-free image. He used independent component analysis (ICA) and a Markov random field (MRF) model for surface estimation. This method could produce impressive results, but unsuitable for heavy haze images and the assumption may become invalid [15]. Related to the Tan method [22], Kratz and Nishino [24] proposed a factorial Markov random field (FMRF) for estimating the scene albedo and depth from a single degraded image. Nishino *et al.* [25] proposed a Bayesian defogging for a similar purpose. Their methods could achieve a good dehazed image but retain some artifacts in infinite-depth regions [15].

The other single-image dehazing method was proposed by He *et al.* [26] through a dark channel prior (DCP) algorithm to fit out a shortcoming of both Tan and Fattal methods [15], [22], [23]. The DCP method realized the dark pixel principle with the atmospherical scattering model and the transmission map function is approximated by the dark channel of the image [1], [15], [19]. The principle of the DCP is that the haze-free image has at least one color channel with a very low intensity close to zero and it can be used to estimate the atmospheric light and transmission map function [1], [15], [26]–[28]. Many improvements in image dehazing method based on DCP have been proposed using many approaches, such as edge-preserving smoothing, bilateral filtering, trilateral filter, guided image filtering, smooth filtering, anisotropic diffusion, window adaptive method, associative filter, mean filters, mean shift filtering, adaptively subdivided quadtree, interpolated filter, Wiener filter, gamma correction, fuzzy theory, and a fusion strategy that widely to optimize the transmission map. The other methods were proposed using dual transformation maps [29], color attenuation prior [30], morphological reconstruction [31], and adaptive air light refinement [32]. The DCP principle offers a new concept, and its effectiveness in image dehazing makes this method get more attention to be adopted in the majority of recent image dehazing methods [19]. However, there are also deficiencies in this method that require a high computation for transmission map and dehazing an image that contains a majority area because of the inhomogeneous color [33]. Several image dehazing methods are

Based on the background, it shows that image dehazing is still a challenging research field to produce better quality images that finally can help computer vision tasks for getting useful information from hazy images. Image dehazing usually produces a smoothed dehazed image that obscures the edge so the image appears blurry. Considering the simplicity and effectiveness of the DCP method, this study proposes to enhance the transmission map by utilizing the normalized Gaussian filtering on the gradient image based on DCP to sharpen the edge. The image gradient represents a directional change in image intensity or measures the change of pixel intensity in a certain direction. Computing the image gradient will detect the edges that

represent the detail of the image. These edges are then used to utilize the detail enhancement on the DCP method. To achieve this objective, Gaussian filtering will be proposed in this study as the preprocessing phase before applying the dehazing based on the DCP method. Moreover, the main contributions of this research are: i) evaluating the use of the Gaussian filter to sharpen the image edges of the hazy images to improve the de-hazing process quality; and ii) reconstructing the de-hazed image based on the gradient of the Gaussian filtered hazy image.

This article is presented in several sections to demonstrate the proposed method and its performance. The proposed methods including the basic methods of Gaussian and DCP are presented in section 2. Research methods for carrying out experiments, especially the use of datasets and performance evaluation methods are presented in section 3. Experimental results and discussion are presented in section 4 and end with conclusions presented in section 5.

2. PROPOSED METHOD

The hazy image occurs due to bad weather with an accumulation of particles in the atmosphere such as haze and fog, thereby holding up the light scattered in the particles along the transmission between the scene and the image capture medium. Hazy images can reduce the visibility and contrast of digital images taken in adverse weather conditions. Mathematically, if I is the observational hazy image and J is the haze-free image, the forming process of a hazy image is modeled in (1) [20], [25], [27], [34], as:

$$I(x) = J(x)e^{-\beta d(x)} + A(1 - e^{-\beta d(x)}), \quad (1)$$

where x represents the image pixel coordinates, A is the global atmospheric light, β is the coefficient of atmospheric scattering, and d is the level of scene depth. The term $e^{-\beta d(x)}$ represents a transmission map, which is formulated as $t(x)$ in (2) [20]:

$$t(x) = e^{-\beta d(x)} \quad (2)$$

In good or clear weather, the coefficient β is 0, so it will get an image I close to the image J or $I \cong J$. Conversely, in hazy weather, the coefficient β cannot be ignored or $\beta \neq 0$. The first term in (1), i.e., $J(x)t(x)$, is called direct attenuation which decreases as the depth of the scene increases. The second term in (1), that is $A(1 - t(x))$, is called the atmospheric light which increases as the depth of the scene increases. Image dehazing is introduced to recover image J from the hazy image I in (3) based on the estimated values of A and t [20] as (3).

$$J(x) = \frac{I(x)-A}{t(x)} + A. \quad (3)$$

In the dark channel prior approach, the haze-free image is assumed to have dark pixels with an intensity value close to zero in at least one color channel in the images [20], [25], [27], [35], which is defined in (4).

$$J^{dark}(x) = \min_{y \in \Omega} \left(\min_{c \in \{r, g, b\}} J^c(y) \right), \quad (4)$$

where, J^c is the intensity for color channel $c \in \{r, g, b\}$ of the color image and $\Omega(x)$ is the local patch centered at pixel x . The minimum value of the three-color channels and all pixels within $\Omega(x)$ are selected as the dark channel $J^{dark}(x)$. The low intensity in the dark channel has three features, namely: i) shadows, ii) surfaces, and iii) dark objects. So, the pixel in the dark channel can be estimated to have a value close to 0 or $J^{dark}(x) \rightarrow 0$ and is called dark channel prior (DCP) [20], [27]. Conversely, the dark channel of a blurred image produces pixels above zero.

The atmospheric light tends to be bright, and the incorporation of atmospheric light and direct attenuation can significantly increase the minimum value of the three-color channel in the local spot. This means that the dark channel pixel values can be an important signal for estimating the haze density. Based on the formula in (1), the local patch minimum intensity for the color channel can be obtained in (5) [20], [36]:

$$\min_{y \in \Omega(x)} \frac{I^c(y)}{A^c} = t(x) \frac{J^c(x)}{A^c} + (1 - t(x)). \quad (5)$$

The local path $\Omega(x)$ is assumed to be constant and is represented as $t(x)$. Then the minimum values of the three-color channels are applied in (6):

$$\min_{y \in \Omega(x)} \frac{I^c(y)}{A^c} = \tilde{t}(x) \min_{y \in \Omega(x)} \left(\min_{y \in \Omega(x)} \frac{I^c(x)}{A^c} \right) + (1 - \tilde{t}(x)). \quad (6)$$

Based on the estimated DCP value, that is $J^{dark}(x) \rightarrow 0$, the $\tilde{t}(x)$ can be represented in (7) [25], [27]:

$$\tilde{t}(x) = 1 - \omega \min_{y \in \Omega(x)} \left(\min_c \frac{I^c(y)}{A^c} \right), \quad (7)$$

where, $\omega \in [0, 1]$ is a parameter used to maintain a certain depth of field so that the image is more natural and realistic. The presence of haze in the image can be assumed to be a noise that comes randomly. The Gaussian filtering technique itself is one of the popular techniques for edge detection and noise reduction caused by low illumination or transmission [37]. Gaussian filtering works with a Gaussian kernel based on the Gaussian distribution function to determine the weights in the kernel to calculate the weighted average of neighboring pixels in an image. With the Gaussian filtering preprocessing, it is expected to get better material input for the dehazing technique because a part of the hazes has been reduced. The Gaussian kernel in ND dimension is formulated in (8) [38],

$$G_{ND}(\tilde{x}, a) = \frac{1}{(\sigma\sqrt{2\pi})^N} e^{-\frac{|\tilde{x}|^2}{2\sigma^2}}, \quad (8)$$

where, \tilde{x} is the vector in N dimension and σ is the standard deviation of Gaussian distribution. In the $2D$ distribution, which is commonly for image processing, the Gaussian function has the form as shown in (9) [39].

$$G_{2D}(\tilde{x}, \tilde{y}, a) = \frac{1}{(\sigma\sqrt{2\pi})^N} e^{-\frac{x^2+y^2}{2\sigma^2}}. \quad (9)$$

The Gaussian filter is generally used for image smoothing by weighting the pixels in the neighborhood around the Gaussian kernel. In image processing, the Gaussian filters have advantages in smoothness, robustness, and efficiency. This filter is very useful for image enhancement such as image denoising and image sharpening, and also edge detection. So, using the Gaussian filter will take many effects at once. Regarding the use of the Gaussian filtering in image dehazing, the Gaussian filter is expected could reduce the noise on the raw hazy image. However, as the Gaussian filter works based on the convolution technique [40], it will produce a blur or smooth image, which will reduce the edge information [41]. The standard deviation and the image padding can be used to control the degree of smoothing [34]. There are many image padding types, such as circular repetition of elements within the dimension, repeating border elements of an array, or symmetric with mirror reflections of itself.

As the Gaussian produces a weighted average of each pixel's neighborhood toward the central pixel value, it will provide soft smoothing and preserve the edges [35]. The Gaussian filter is also invariant in the gray-level image, where the normalization coefficient is $1/2\pi^2$ as formulated in (9) remains the gray level average on the blurred image [39]. The original and the hazy images itself are shown in Figure 1(a) and Figure 1(b). Figure 1(c) shows an example of the Gaussian filtering for the hazy image enhancement. It shows that the use of a Gaussian filter could enhance the quality of hazy images. The filtered hazy image looks smooth with less noise and still retains the image detail. Based on the Gaussian filter performances, this study proposes the use of Gaussian to enhance the raw hazy image quality before it is dehazed using the DCP.

Figure 2 shows the experiment stages that are designed into several steps. The first step is input preprocessing. In this step, the hazy image input is filtered by Gaussian filtering. As the Gaussian is a smoothing kernel, it will produce a smooth image and may reduce the detail. The image padding and the standard deviation can be used to control the smoothness to avoid losing more of the image detail. The next step is finding the dark channel of the hazy image by selecting the minimum pixels in the gray level guided by the selected window size. The next step is computing the gradient both the magnitude and direction. This gradient is then used for finding the sky region, which will be used to estimate the atmospheric light and transmission map. Those estimations will be used to reconstruct the dehazed image using the atmospherical light and transmission map estimation. Finally, the hazy and dehazed images will be evaluated using peak-signal-to-noise-ratio (PSNR) and structural index similarity (SSIM) compared to the ground-truth images.

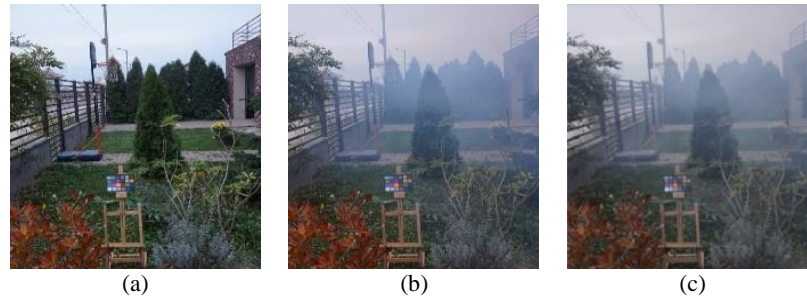


Figure 1. Gaussian filter example of (a) original haze-free image, (b) original hazy image (PSNR=15.61 dB), and (c) filtered hazy image (PSNR= 33.24 dB, image padding=circular)

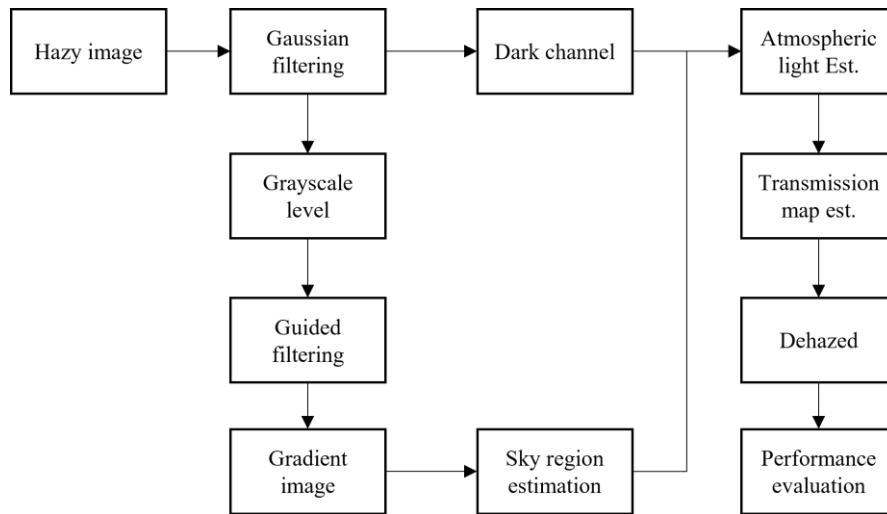


Figure 2. Experimental stages diagram for the proposed method

3. RESEARCH METHOD

3.1. Experimental dataset

This experiment uses a public outdoor scene dataset, namely the O-HAZE dataset, which is a dehazing benchmark with real hazy and haze-free outdoor images captured under the same illumination parameters [36], [42]. This dataset contains 45 pairs of hazy and haze-free images and it can be downloaded at the URL: <https://data.vision.ee.ethz.ch/cvl/ntire18/o-haze/>. This dataset has been introduced by Ancuti *et al.* [36] for a comparative study of state-of-the-art dehazing techniques. However, due to similar analysis on each image in this article, this experiment was only carried out on the first four hazy images of the dataset as a sample analysis, which are *oh1.png*, *oh2.png*, *oh3.png*, and *oh4.png*. Figures 3(a)-3(d) shows the hazy images, while Figures 3(e)-3(h) shows the ground-truth images that are used in this experiment.

3.2. Performances evaluation method

The performance evaluation of the proposed method is measured by the PSNR and SSIM metrics. The PSNR is an image quality metric that compares the pixel values of the original image to the processed image due to the occurrence of some changes or transformations to the original image. This PSNR is computed by calculating the ratio between the maximum signal power and the power of the distorting noise, which is measured using mean squared error (MSE). The PSNR is a logarithm term of the decibel scale and has units of decibels (dB). A higher value of PSNR indicates that the processed image is close to the original image. Suppose x is an original image with $M \times N$ and y is the processed image with $M \times N$ of size, max is the maximum of the signal scale, M is the number of rows, and N is the number of columns. The PSNR between x and y is then formulated in (10) [39], [42]–[44].

$$PSNR_{(x,y)} = \frac{10 \log_{10}(max^2)}{\frac{1}{M \times N} \sum_{i=1}^M \sum_{j=1}^N (x_{i,j} - y_{i,j})^2} \quad (10)$$

The SSIM metric is an image quality metric that compares the luminance, contrast, and structure of the original image to the distorted image. The SSIM metric is also known as the two-image similarity index that assesses the visual impact of an image after processing. Suppose x is an original image with $M \times N$ of size and y is a processed image with $M \times N$ of size, the SSIM value between x and y is formulated in (11) [39], [42]–[45] as,

$$\text{SSIM}_{(x,y)} = [l(x,y)]^\alpha [c(x,y)]^\beta [s(x,y)]^\gamma \quad (11)$$

$$l(x,y) = \frac{2\mu_x\mu_y + C_1}{2\mu_x^2 + \mu_y^2 + C_1} \quad (12)$$

$$c(x,y) = \frac{2\sigma_x\sigma_y + C_2}{2\sigma_x^2 + \sigma_y^2 + C_2} \quad (13)$$

$$s(x,y) = \frac{\sigma_{xy} + C_3}{\sigma_x\sigma_y + C_3} \quad (14)$$

with μ_x and μ_y are the local means of image x and y , σ_x and σ_y are the deviation standards of images x and y , σ_{xy} is a cross-covariance between x and y , and C_1 , C_2 , and C_3 are the regularization constants for the luminance $l(x,y)$, contrast $c(x,y)$, and structural $s(x,y)$ terms, which are formulated in (12), (13), and (14), respectively. As with PSNR, a higher SSIM value indicates that the processed image has a similar image structure to the original image.

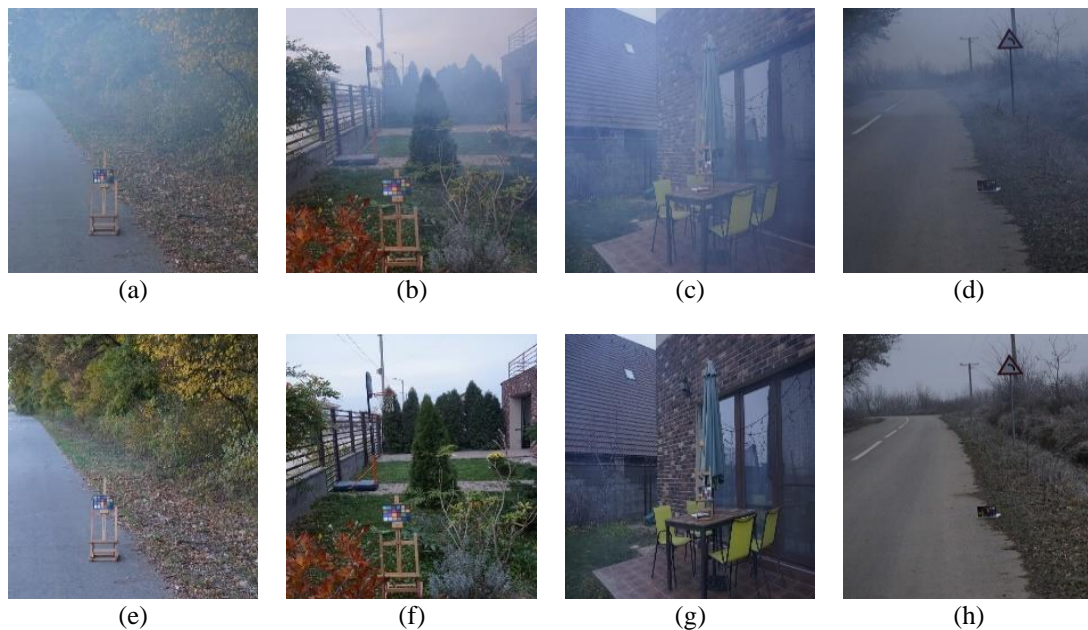


Figure 3. Hazy images dataset of (a) oh1_hazy.png, (b) oh2_hazy.png, (c) oh3_hazy.png, and (d) oh4_hazy.png; and ground truth images: (e) oh1.png, (f) oh2.png, (g) oh3.png, and (h) oh4.png

4. RESULTS AND DISCUSSION

The first experiment performs image preprocessing on an image dataset by applying Gaussian filtering. Each value in a Gaussian filter comes from a zero-mean Gaussian distribution with a standard deviation that can be adjusted in size. Figures 4(a) to 4(d) show the histogram images comparison before and after filtering for each hazy image. Based on the histograms, some numbers of pixels are corrected and are expected to have an impact on the haze reduction process. The PSNR values of oh1_hazy.png, oh2_hazy.png, oh3_hazy.png, and oh4_hazy.png before filtering are 14.68, 15.61, 14.99, and 21.76 dB, respectively. After filtering, the PSNR values become increased to 14.83, 15.61, 15.16, and 22.07 dB, respectively. Figures 5(a) to 5(d) show the visual quality of the hazy images after Gaussian filtering. There is a bit of imperceptible improvement after filtering that provides different visual impacts, such as sharpening, brightness, and blur.

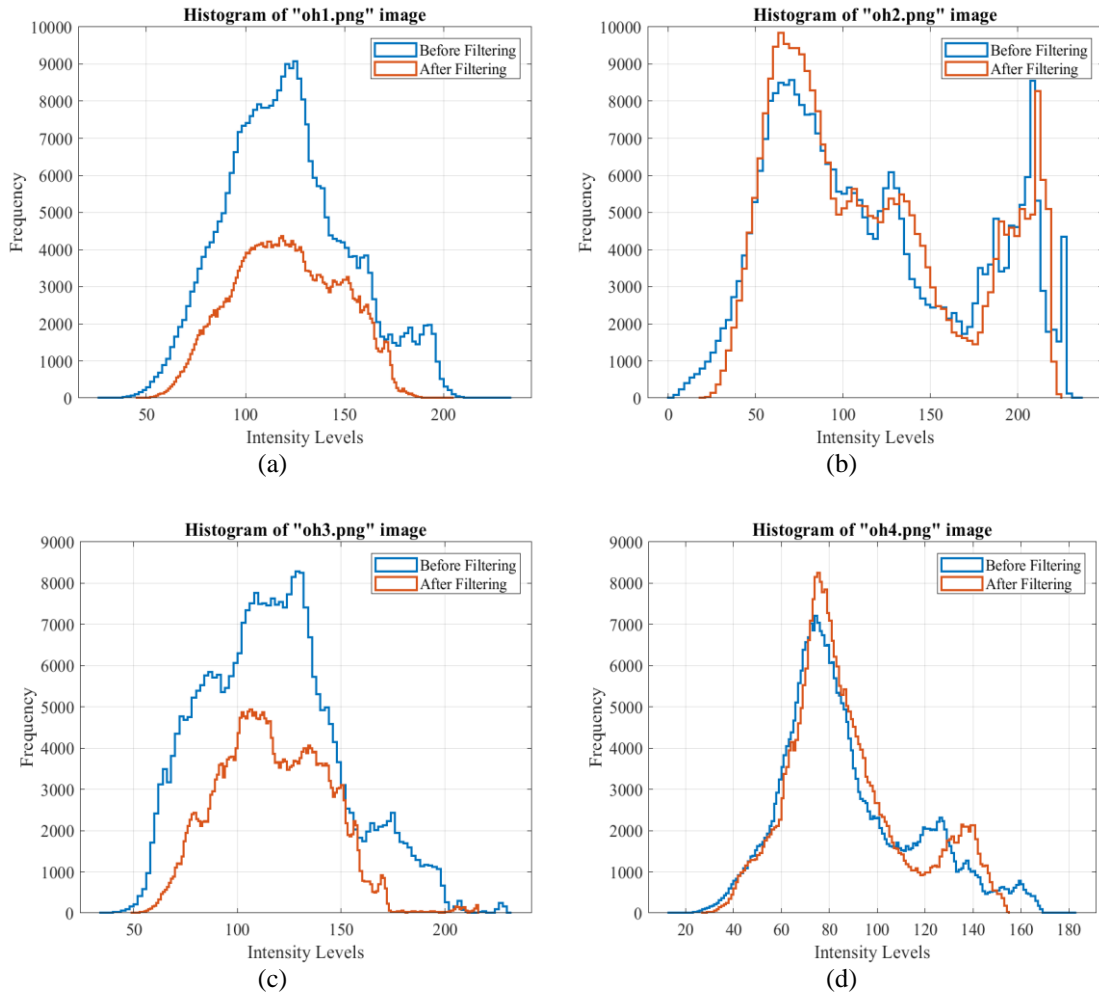


Figure 4. The haze image histogram before (blue color) and after filtering (red color): (a) oh1_hazy.png, (b) oh2_hazy.png, (c) oh3_hazy.png, and (d) oh4_hazy.png

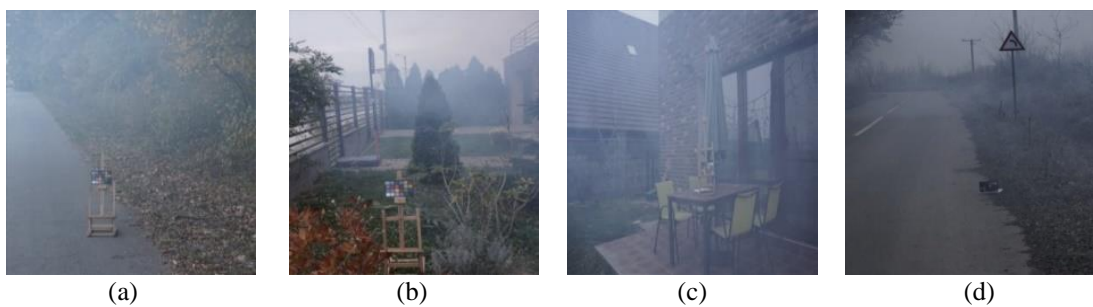


Figure 5. The visual quality of the hazy images after Gaussian filtering of (a) oh1_hazy.png, (b) oh2_hazy.png, (c) oh3_hazy.png, and (c) oh3_hazy.png

The next step of this experiment is the main processing for hazy image reduction using a guided filtering method based on DCP. This step consists of several processes, such as dark channel transformation, atmospheric estimation, minimization of dark channel filter, and finally applying guided filtering for dehazed image reconstruction. The dark channel transformation aims to capture images with dark intensity. As is known, a haze-free outdoor image has the special characteristic that it has dark pixels with an intensity value close to zero in at least one-color channel in the image. There is a window size parameter should be used to take the dark intensity. Figures 6(a) to 6(d) show the dark channel of the hazy images by selecting the window size of 7 of the dataset images represented on the right side. The pixel values of these dark channels

for all hazy images are in the range of [0.11; 0.58], [0.01; 0.82], [0.14; 0.76], and [0.05; 0.51], with deviation standards 0.016, 0.03, 0.02, and 0.03, respectively. These dark channel images are then optimized by minimum filtering to take the smallest intensity level of the dark channel.

Finding the gradient of the hazy gray level image is then performed to identify the sky region. The gradient magnitude is then processed by guided filtering to refine the new and smoothed gradient by median filtering. In this experiment, the gradient is computed by an intermediate method with the gradient magnitude and gradient direction. Figures 7(a) to 7(d) show the both gradient magnitude and gradient directions of all hazy images.

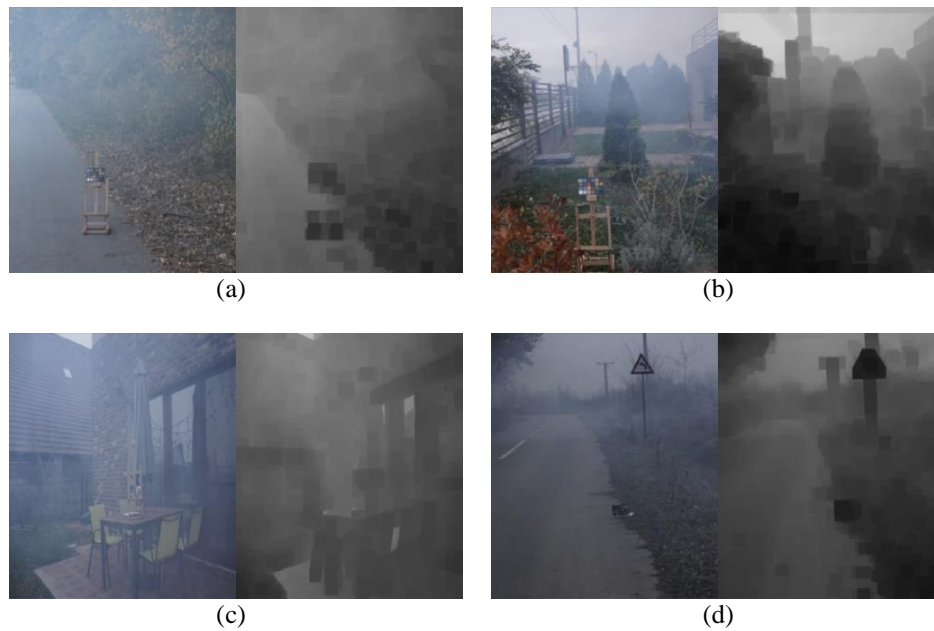


Figure. 6 Original hazy images (left) and dark channel images (right) of (a) oh1_hazy.png, (b) oh2_hazy.png, (c) oh3_hazy.png, and (d) oh4_hazy.png

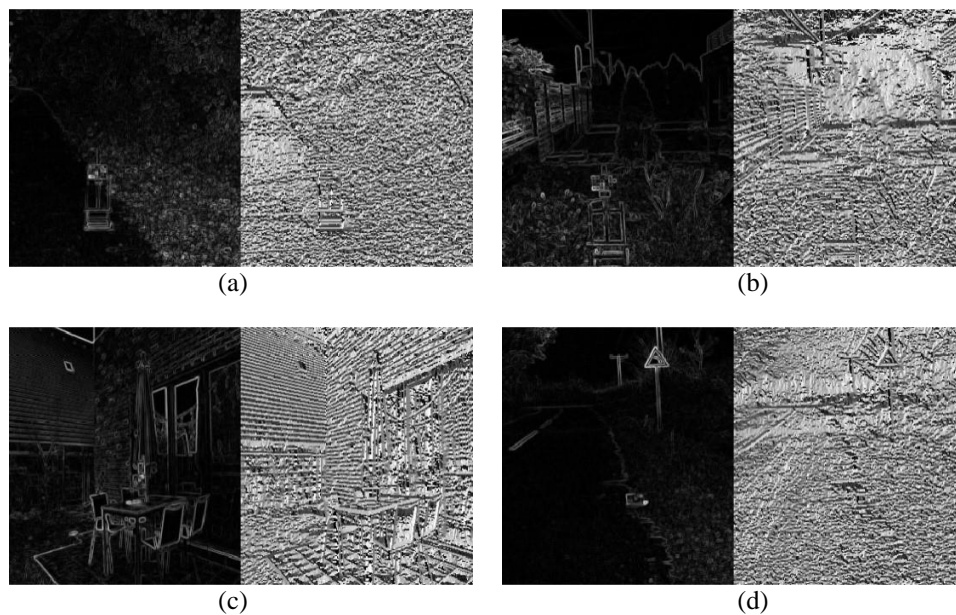


Figure 7. Gradient magnitude (left) and gradient direction (right) on the gray level of (a) oh1_hazy.png, (b) oh2_hazy.png, (c) oh3_hazy.png, and (d) oh4_hazy.png

The sky region is then obtained by thresholding based on this gradient magnitude. The gradient pixel values below 0.01 are then assigned as the black pixels, conversely assigned to the white pixels. Figures 8(a) to 8(d) show the selected sky region results of the hazy images shown on the right side. The sky region images are then used to estimate the atmospheric light and transmission map. Atmospheric light is estimated from the dark channel based on local patches. If the size of the local patch is insufficient then the largest local patch is used to estimate atmospheric light.

Next, atmospheric light estimation is carried out using the pixel with the highest dark pixel value. If there is a brightly shining object, it can be filtered with local entropy. The atmospheric transmission map estimation is started by building a transmission matrix. This matrix is computed by dividing the difference value of the dark channel by the maximum value of the dark pixels weighted by the parameter $0 \leq \omega \leq 1$ of the average value of the dark channel pixels. Figures 9(a) to 9(d) show the transmission map results using $\omega = 0.9$.



Figure 8. Hazy image (left) and sky region (right) of (a) oh1_hazy.png, (b) oh2_hazy.png, (c) oh3_hazy.png, and (d) oh4_hazy.png

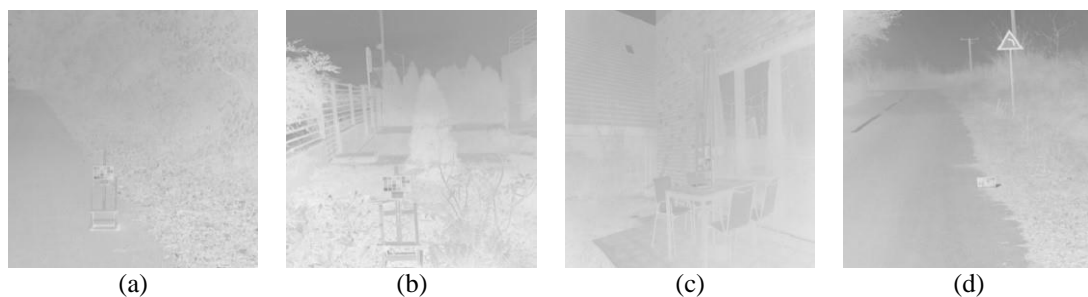


Figure 9. Transmission map estimation of (a) oh1_hazy.png, (b) oh2_hazy.png, (c) oh3_hazy.png, and (d) oh4_hazy.png

The final step is reconstructing the dehazed image by atmospheric light and transmission map. The dehazed image can be carried out with the direct attenuation term as the transmission $t(x)$ is closest to zero. This reconstruction also uses a transmission map threshold to prevent the image pixel value from becoming too large when the projection map is very small. The threshold value is chosen to be a small threshold pixel value to prevent the overall transition to the white point. For pixel values less than the threshold value then it can be assigned closer to that threshold value. Figures 10(a) to 10(d) shows the reconstruction results of all hazy images with a threshold of 0.1.

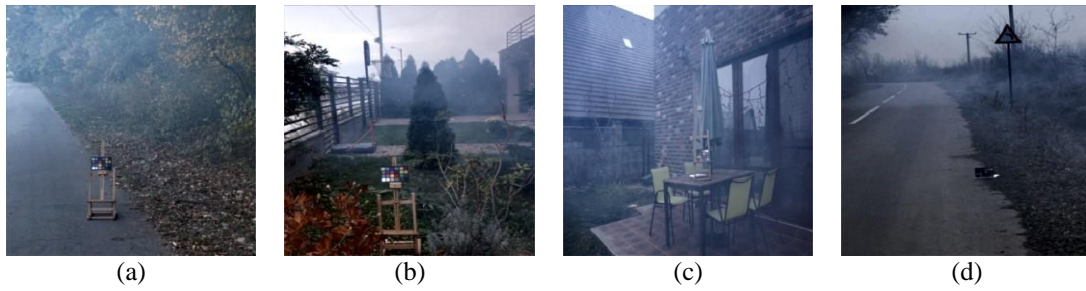


Figure 10. Reconstructed de-hazed image of (a) oh1_hazy.png, (b) oh2_hazy.png, (c) oh3_hazy.png, and (d) oh4_hazy.png

Although the proposed method could not remove haze perfectly, the proposed method could still increase the PSNR and SSIM values for all dataset images compared to the ground truth images. For example, the PSNR of the hazy image oh1.png before the dehazing process is 14.84dB and increases to 15.88dB after the dehazing process. The image similarity of the hazy image oh1.png is also increasing from 44.06% to 48.21%. A similar achievement also occurs in other images, as described in Table 1.

For a visual explanation, Figures 11(a) and 11(b) show the sample areas of the proposed method achievement that are cropped from the hazy and dehazed images. It shows that the dehazed image is more perceptible than the original hazy image. From the cropped area of the dehazed image and then enlarged, it appears that the proposed dehazing method could retain sharper information.

The reconstructed dehazed image quality is influenced by the estimation of the transmission factor. Figures 12(a) and 12(b) shows the PSNR and SSIM distributions of dehazed images with various transmission factors from 0.1 to 1.0. For the hazy image oh1.png, the mean, median, maximum, and minimum of PSNR are 15.01 dB, 15.06 dB, 15.20 dB, and 14.63 dB, respectively. For the hazy image oh2.png, the mean, median, maximum, and minimum of PSNR are 17.47 dB, 17.63 dB, 18.21 dB, and 16.28 dB, respectively. For the hazy image oh3.png, the mean, median, maximum, and minimum of PSNR are 16.89 dB, 16.79 dB, 18.97 dB, and 15.09 dB, respectively. While for the hazy image oh4.png, the mean, median, maximum, and minimum of PSNR are 21.73 dB, 21.97 dB, 23.21 dB, and 19.54 dB, respectively. For SSIM distributions, the oh1.png has mean, median, maximum, and minimum of SSIM about 49.84%, 50.42%, 50.93%, and 46.94%, respectively. For the hazy image oh2.png, the mean, median, maximum, and minimum of SSIM are 69.46%, 70.38%, 71.33%, and 64.82%, respectively. For the hazy image oh3.png, the mean, median, maximum, and minimum of SSIM are 75.21%, 75.30%, 75.86%, and 74.20%, respectively. Whereas, for the hazy image oh4.png, the mean, median, maximum, and minimum of PSNR are 70.44%, 71.14%, 75.24%, and 63.52%, respectively.

Table 1. Performance evaluation of the proposed method

Input Image	PSNR			SSIM (%)		
	Hazy	Dehazed	Deviation	Hazy	Dehazed	Deviation
oh1_hazy	14.84	15.88	1.04	44.06	48.21	4.15
oh2_hazy	15.52	18.21	2.59	63.12	66.69	3.57
oh3_hazy	15.17	18.49	3.32	69.76	75.18	5.42
oh4_hazy	22.07	23.18	1.11	70/70	76.77	6.07

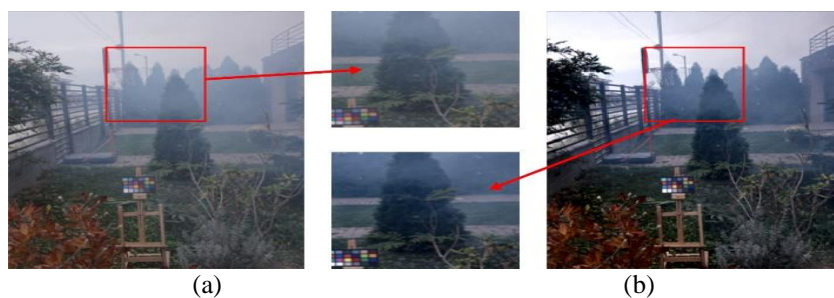


Figure 11. Details of the visual quality enhancement for oh2.png image before de-hazing (a) and after de-hazing and (b) using the proposed method

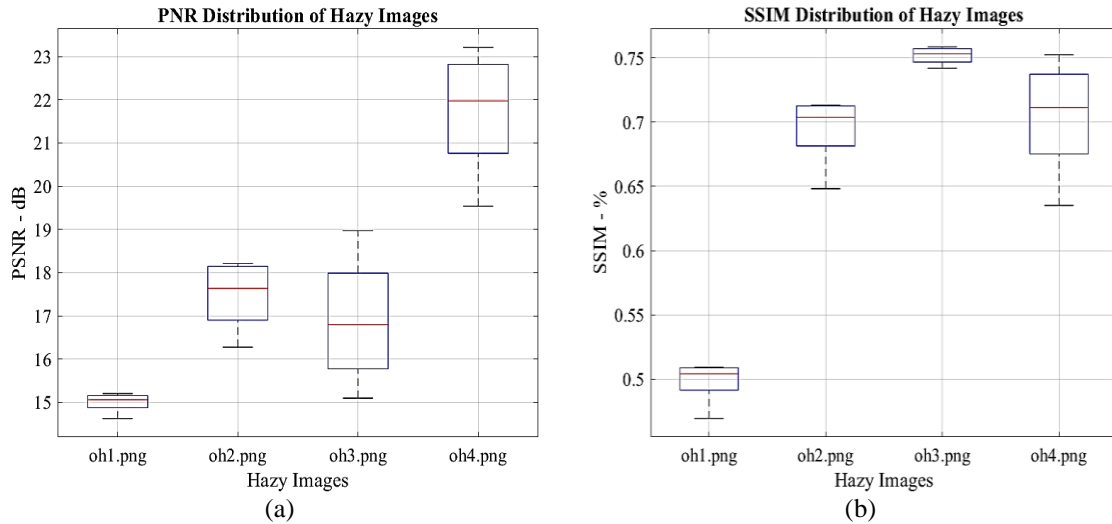


Figure 12. Distribution of (a) PSNR and (b) SSIM values on various transmission maps ω in $[0,1]$

To strengthen validation, the proposed method is compared with other existing similar methods in single image dehazing, which are introduced by Ehsan *et al.* [29], Zhu *et al.* [30], He *et al.* [26], Colores *et al.* [31], and Dhara *et al.* [32]. For comparison purposes, this experiment uses the house.png image, which is used in the performance evaluation of their methods. The ground-truth and hazy images are shown in Figures 13(a) and 13(b), respectively. The Gaussian filtered and the dark channel images are shown in Figures 13(c) and 13(d) respectively. The gradient and the sky region images are shown in Figures 13(e) and 13(f), respectively. The transmission map and the reconstructed dehazed images are shown in Figures 13(g) and 13(h), respectively. After applying the proposed method, the dehazed image has 16.47 dB of PSNR. This achievement shows a visual quality enhancement of the hazy image which previously had a PSNR value of 14.74 dB compared to the ground-truth haze-free image. Based on this PSNR, the proposed method outperforms the other methods in Ehsan *et al.* [29], Zhu *et al.* [30], He *et al.* [26], Colores *et al.* [31], and Dhara *et al.* [32], where their PSNR values are 14.96 dB, 11.97 dB, 14.19 dB, 9.49 dB, and 13.38 dB, respectively [29].

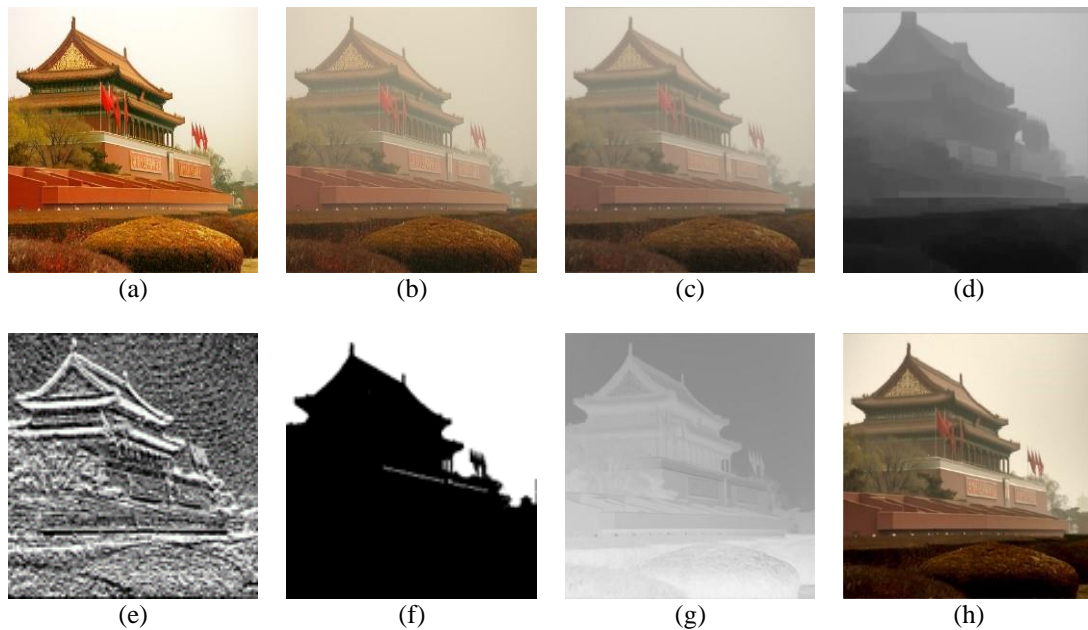


Figure 13. The house.png test image of (a) ground-truth, (b) hazy, (c) Gaussian filtered, (d) dark channel, (e) gradient, (f) sky region, (g) transmission, and (h) de-hazed

5. CONCLUSION

Joining the Gaussian filter with the DCP method for image dehazing has been introduced in this paper. The Gaussian characteristics, which are efficient, robust, and smooth, can help the DCP image dehazing method in taking recovered dehazed images. Although could not recover the haze-free image perfectly, the proposed method could still take the dehazed images with better visual quality and similarity compared to the common recent DCP methods. It can be tolerated as the Gaussian filter provides a non-contrast effect. This filter was still able to retain the edge detail which is very useful for recovering the dehazed image, but this filter also blurs the image surface which can reduce the strength of the edge detail. Further studies need to be carried out to overcome challenges related to the use of DCP in image dehazing, such as finding the best gradient, utilizing weight factors in the atmospheric light and transmission estimation process, as well as finding better dark images and sky regions.

ACKNOWLEDGEMENTS

The authors would like to thank the Postgraduate School, Diponegoro University for providing financial support to this research through the fundamental research grant for 2023's fiscal year.

REFERENCES

- [1] G. H. Babu and N. Venkatram, "A survey on analysis and implementation of state-of-the-art haze removal techniques," *Journal of Visual Communication and Image Representation*, vol. 72, no. October 2019, 2020, doi: 10.1016/j.jvcir.2020.102912.
- [2] T. Van Nguyen, A. G. Vien, and C. Lee, "Real-time image and video dehazing based on multiscale guided filtering," *Multimedia Tools and Applications*, vol. 81, pp. 36567–36584, 2022, doi: 10.1007/s11042-022-13533-4.
- [3] Y. Liu, P. Jia, H. Zhou, and A. Wang, "Joint dehazing and denoising for single nighttime image via multi-scale decomposition," *Multimedia Tools and Applications*, vol. 81, no. 17, pp. 23941–23962, 2022, doi: 10.1007/s11042-022-12681-x.
- [4] T. R. V. Lakshmi, C. V. K. Reddy, K. Padmavathi, K. Swaraja, and K. Meenakshi, "Entropy based single image dehazing with refined transmission using holistic edges," *Multimedia Tools and Applications*, vol. 81, no. 14, pp. 20229–20253, 2022, doi: 10.1007/s11042-022-12485-z.
- [5] S. J. Kamble and M. R. Kounte, "Application of improved you only look once model in road traffic monitoring system," *International Journal of Electrical and Computer Engineering*, vol. 13, no. 4, pp. 4612–4622, 2023, doi: 10.11591/ijece.v13i4.pp4612-4622.
- [6] F. Martínez, H. Montiel, and F. Martínez, "Comparative study of optimization algorithms on convolutional network for autonomous driving," *International Journal of Electrical and Computer Engineering*, vol. 12, no. 6, pp. 6363–6372, 2022, doi: 10.11591/ijece.v12i6.pp6363-6372.
- [7] E. A. Mahareek, E. K. Elsayed, N. M. ElDesouky, and K. A. Eldahshan, "Detecting anomalies in security cameras with 3D-convolutional neural network and convolutional long short-term memory," *International Journal of Electrical and Computer Engineering*, vol. 14, no. 1, pp. 993–1004, 2024, doi: 10.11591/ijece.v14i1.pp993-1004.
- [8] D. Ngo, S. Lee, Q. H. Nguyen, T. M. Ngo, G. D. Lee, and B. Kang, "Single image haze removal from image enhancement perspective for real-time vision-based systems," *Sensors (Switzerland)*, vol. 20, no. 18, pp. 1–23, 2020, doi: 10.3390/s20185170.
- [9] S. Banerjee and S. S. Chaudhuri, "Bacterial foraging-fuzzy synergism based image dehazing," *Multimedia Tools and Applications*, vol. 80, no. 6, pp. 8377–8421, 2021, doi: 10.1007/s11042-020-09794-6.
- [10] Y. Y. Schechner, S. G. Narasimhan, and S. K. Nayar, "Instant dehazing of images using polarization," in *Proceeding of the IEEE Computer Society Conference on Computer Vision and Pattern Recognition*, 2001, pp. 325–332, doi: 10.1109/cvpr.2001.990493.
- [11] Z. I. Azhari, S. Setumin, E. Noorsal, and M. H. Abdullah, "Digital image enhancement by brightness and contrast manipulation using Verilog hardware description language," *International Journal of Electrical and Computer Engineering*, vol. 13, no. 2, pp. 1346–1357, 2023, doi: 10.11591/ijece.v13i2.pp1346-1357.
- [12] S. C. Raikwar and S. Tapaswi, "Lower bound on transmission using non-linear bounding function in single image dehazing," *IEEE Transactions on Image Processing*, vol. 29, pp. 4832–4847, 2020, doi: 10.1109/TIP.2020.2975909.
- [13] J. Guo, J. Syue, V. R. Radzicki, and H. Lee, "An efficient fusion-based defogging," *IEEE Transactions on Image*, vol. 26, no. 9, pp. 4217–4228, 2017.
- [14] S. G. Narasimhan and S. K. Nayar, "Contrast restoration of weather degraded images," *IEEE Transactions on Pattern Analysis and Machine Intelligence*, vol. 25, no. 6, pp. 713–724, 2003, doi: 10.1109/TPAMI.2003.1201821.
- [15] W. Wang and X. Yuan, "Recent advances in image dehazing," *IEEE/CAA Journal of Automatica Sinica*, vol. 4, no. 3, pp. 410–436, 2017, doi: 10.1109/JAS.2017.7510532.
- [16] F. Liu, L. Cao, X. Shao, P. Han, and X. Bin, "Polarimetric dehazing utilizing spatial frequency segregation of images," *Applied Optics*, vol. 54, no. 27, pp. 8116–8122, 2015, doi: 10.1364/ao.54.008116.
- [17] S. Shwartz, E. Namer, and Y. Y. Schechner, "Blind haze separation," in *Proceeding of the IEEE Computer Society Conference on Computer Vision and Pattern Recognition*, 2006, vol. 2, pp. 1984–1991, doi: 10.1109/CVPR.2006.71.
- [18] D. Wu and Q. Dai, "Data-driven visibility enhancement using multi-camera system," in *Proceeding of SPIE - The International Society for Optical Engineering*, 2010, vol. 7689, pp. 76890H-1-76890H-12, doi: 10.1117/12.849853.
- [19] S. Lee, S. Yun, J. H. Nam, C. S. Won, and S. W. Jung, "A review on dark channel prior based image dehazing algorithms," *Eurasip Journal on Image and Video Processing*, vol. 2016, pp. 1–23, 2016, doi: 10.1186/s13640-016-0104-y.
- [20] B. Li *et al.*, "Benchmarking single-image dehazing and beyond," *IEEE Transactions on Image Processing*, vol. 28, no. 1, pp. 492–505, 2019, doi: 10.1109/TIP.2018.2867951.
- [21] W. Wang, X. Yuan, X. Wu, and Y. Dong, "An airlight estimation method for image dehazing based on gray projection," *Multimedia Tools and Applications*, vol. 79, no. 37–38, pp. 27185–27203, 2020, doi: 10.1007/s11042-020-09380-w.
- [22] R. T. Tan, "Visibility in bad weather from a Single Image," in *Proceeding of the Computer Vision and Pattern Recognition. CVPR 2008*, 2008, pp. 1–8.

- [23] R. Fattal, "Single image dehazing," *ACM Transactions on Graphics*, vol. 27, no. 3, pp. 72:1-72:9, 2008, doi: 10.1145/1360612.1360671.
- [24] L. Kratz and K. Nishino, "Factorizing scene albedo and depth from a single foggy image," in *Proceeding of the IEEE International Conference on Computer Vision*, 2009, no. November 2009, pp. 1701–1708, doi: 10.1109/ICCV.2009.5459382.
- [25] K. Nishino, L. Kratz, and S. Lombardi, "Bayesian defogging," *International Journal of Computer Vision*, vol. 98, no. 3, pp. 263–278, 2012, doi: 10.1007/s11263-011-0508-1.
- [26] K. He, J. Sun, and X. Tang, "Single image haze removal using dark channel prior," *IEEE Transactions on Pattern Analysis and Machine Intelligence*, vol. 33, no. 12, pp. 2341–2353, 2011, doi: 10.1109/TPAMI.2010.168.
- [27] V. Malathi and A. Manikandan, "An underwater image enhancement by reducing speckle noise using modified anisotropic diffusion filter," *International Journal of Electrical and Computer Engineering*, vol. 13, no. 6, pp. 6361–6368, 2023, doi: 10.11591/ijece.v13i6.pp6361-6368.
- [28] H. A. Ghani *et al.*, "Advances in lane marking detection algorithms for all-weather conditions," *International Journal of Electrical and Computer Engineering*, vol. 11, no. 4, pp. 3365–3373, 2021, doi: 10.11591/ijece.v11i4.pp3365-3373.
- [29] S. M. Ehsan, M. Imran, A. Ullah, and E. Elbasi, "A single image dehazing technique using the dual transmission maps strategy and gradient-domain guided image filtering," *IEEE Access*, vol. 9, pp. 89055–89063, 2021, doi: 10.1109/ACCESS.2021.3090078.
- [30] Q. Zhu, J. Mai, and L. Shao, "A fast single image haze removal algorithm using color attenuation prior," *IEEE Transactions on Image Processing*, vol. 24, no. 11, pp. 3522–3533, 2015, doi: 10.1109/TIP.2015.2446191.
- [31] S. S.-Colores, E. C.-Yepez, J. M. R.-Arreguin, G. Botella, L. M. L.-Carrillo, and S. Ledesma, "A fast image dehazing algorithm using morphological reconstruction," *IEEE Transactions on Image Processing*, vol. 28, no. 5, pp. 2357–2366, 2019, doi: 10.1109/TIP.2018.2885490.
- [32] S. K. Dhara, M. Roy, D. Sen, and P. K. Biswas, "Color cast dependent image dehazing via adaptive airlight refinement and non-linear color balancing," *IEEE Transactions on Circuits and Systems for Video Technology*, vol. 31, no. 5, pp. 2076–2081, 2021, doi: 10.1109/TCSVT.2020.3007850.
- [33] C. Chengtao, Z. Qiuyu, and L. Yanhua, "A survey of image dehazing approaches," in *Proceeding of the 2015 27th Chinese Control and Decision Conference, CCDC 2015*, 2015, pp. 3964–3969, doi: 10.1109/CCDC.2015.7162616.
- [34] R. Fisher, S. Perkins, A. Walker, and E. Wolfart, "Gaussian Smoothing," *Filtering*, 2016.
- [35] B. H. Chen, Y. S. Tseng, and J. L. Yin, "Gaussian-adaptive bilateral filter," *IEEE Signal Processing Letters*, vol. 27, pp. 1670–1674, 2020, doi: 10.1109/LSP.2020.3024990.
- [36] C. O. Ancuti, C. Ancuti, R. Timofte, and C. De Vleeschouwer, "O-HAZE: A dehazing benchmark with real hazy and haze-free outdoor images," *IEEE Computer Society Conference on Computer Vision and Pattern Recognition Workshops*, vol. 2018-June, pp. 867–875, 2018, doi: 10.1109/CVPRW.2018.00119.
- [37] F. Yuan, Y. Zhou, X. Xia, X. Qian, and J. Huang, "A confidence prior for image dehazing," *Pattern Recognition*, vol. 119, p. 108076, 2021, doi: 10.1016/j.patcog.2021.108076.
- [38] M. K. Chung, "Gaussian kernel smoothing," *Statistical and Computational Methods in Brain Image Analysis*, pp. 69–84, 2018, doi: 10.1201/b15056-6.
- [39] J. Peng *et al.*, "Implementation of the structural SIMilarity (SSIM) index as a quantitative evaluation tool for dose distribution error detection," *Medical Physics*, vol. 47, no. 4, pp. 1907–1919, 2020, doi: 10.1002/mp.14010.
- [40] Kusriani, M. R. A. Yudianto, and H. Al Fatta, "The effect of Gaussian filter and data preprocessing on the classification of Punakawan puppet images with the convolutional neural network algorithm," *International Journal of Electrical and Computer Engineering*, vol. 12, no. 4, pp. 3752–3761, 2022, doi: 10.11591/ijece.v12i4.pp3752-3761.
- [41] H. Fu, W. Liu, H. Chen, and Z. Wang, "An anisotropic Gaussian filtering model for image de-hazing," *IEEE Access*, vol. 8, pp. 175140–175149, 2020, doi: 10.1109/ACCESS.2020.3026185.
- [42] Y. Yang, Z. Wang, W. Hong, and H. Yue, "Single image dehazing algorithm based on double exponential attenuation model," *Multimedia Tools and Applications*, vol. 80, no. 10, pp. 15701–15718, 2021, doi: 10.1007/s11042-021-10540-9.
- [43] A. Marjuni and O. D. Nurhayati, "Robustness improvement against a nongGeometrical attacks of lifting scheme-based image watermarking through singular value and Schur decompositions," *International Journal of Intelligent Engineering and Systems*, vol. 14, no. 4, pp. 217–230, 2021, doi: 10.22266/ijies2021.0831.20.
- [44] N. R. Hamza, R. A. Dihin, and M. H. Abdulameer, "A hybrid image similarity measure based on a new combination of different similarity techniques," *International Journal of Electrical and Computer Engineering*, vol. 10, no. 2, pp. 1814–1822, 2020, doi: 10.11591/ijece.v10i2.pp1814-1822.
- [45] P. P. Babu, T. J. Prasad, and K. Soundararajan, "Image compression and reconstruction using improved Stockwell transform for quality enhancement," *International Journal of Electrical and Computer Engineering*, vol. 14, no. 2, pp. 1583–1593, 2024, doi: 10.11591/ijece.v14i2.pp1583-1593.

BIOGRAPHIES OF AUTHORS



Oky Dwi Nurhayati    received a bachelor's degree in electrical engineering from Institut Teknologi Telkom, Indonesia in 2002 and master's and doctoral degrees in electrical engineering and information technology from Gadjah Mada University, Indonesia in 2008 and 2011, respectively. Currently, she is an Associate Professor at the Department of Computer Engineering, Faculty of Engineering, Diponegoro University. She is also a lecturer at the Master and Doctorate Program of Information Systems, Postgraduate School, Diponegoro University. Her research interests include multimedia and computer vision, software engineering, computer engineering, image processing, speech recognition, information systems, security systems, data mining, big data, machine learning, fuzzy systems, and artificial intelligence. She can be contacted at email: okydw@gmail.com.



Bayu Surarso    received a bachelor's degree in mathematics from Gadjah Mada University, Indonesia in 1987 and master's and doctoral degrees from Hiroshima University, Japan in 1995 and 1998, respectively. Currently, he is an associate professor at the Department of Computer Engineering, Faculty of Engineering, Diponegoro University. He is also a lecturer at the Master Program of Information Systems, Postgraduate School, Diponegoro University. His research interests include mathematics, information systems, decision support systems, security and cryptography, image processing, machine learning, data mining, fuzzy systems, optimization techniques, forecasting techniques, and artificial intelligence. He can be contacted at email: bayusurarlo@yahoo.com.



Wahyul Amien Syafei    received a bachelor's degree from Diponegoro University, Indonesia in 1995, a master's degree from Sepuluh Nopember Institute of Technology, Indonesia in 2002, and a doctoral degree from Kyushu Institute of Technology, Japan in 2010. Currently, he is an associate professor at the Master Program of Electrical Engineering, Faculty of Engineering, Diponegoro University. He is also a lecturer at the Master Program of Electrical Engineering, Postgraduate School, Diponegoro University. His research interests include transmission channels, digital communication systems, multimedia, multimedia networks, computer graphics, data communication, wireless and mobile networks, multimedia telecommunication, information systems, and signal transformation processing. He can be contacted at email: wasyafe@gmail.com.



Dinar Mutiara Kusumo Nugraheni    received a bachelor's degree from Diponegoro University, Indonesia in 2002, and master's and Doctoral degrees from Flinders University, Adelaide, South Australia in 2008 and 2019, respectively. Currently, she is an associate professor at the bachelor Program of Informatics, Faculty of Science and Mathematics, Diponegoro University. He is also a lecturer at the Master Program of Information Systems, Postgraduate School, Diponegoro University. Her research interests include information systems, software engineering, human and computer interaction, project management, database, system engineering, and information technology. She can be contacted at email: dinar.mutiara@live.undip.ac.id.